water

MDPI

Article

Assessment of Climate Change and Associated Vegetation Cover Change on Watershed-Scale Runoff and Sediment Yield

Shanghong Zhang *, Zehao Li, Xiaonan Lin and Cheng Zhang

Renewable Energy School, North China Electric Power University, Beijing 102206, China
* Correspondence: zhangsh928@126.com; Tel.: +86-10-61772405; Fax: +86-10-61772234

Received: 5 June 2019; Accepted: 2 July 2019; Published: 4 July 2019

check for updates

Abstract: Climate change has an important impact on water balance and material circulation in watersheds. Quantifying the influence of climate and climate-driven vegetation cover changes on watershed-scale runoff and sediment yield will help to deepen our understanding of the environmental effects of climate change. Taking the Zhenjiangguan Watershed in Sichuan Province, China as a case study, three downscaled general circulation models with two emission scenarios were used to generate possible climatic conditions for three future periods of P1 (2020–2039), P2 (2050–2069) and P3 (2080–2099). Differences in scenarios were compared with the base period 1980–1999. Then, a Normalized Difference Vegetation Index climate factor regression model was established to analyze changes to vegetation cover under the climate change scenarios. Finally, a Soil and Water Assessment Tool model was built to simulate the response of runoff and sediment yield in the three future periods under two different scenarios: only changes in climate and synergistic changes in climate and vegetation cover. The temperature and precipitation projections showed a significant increasing trend compared to the baseline condition for both emission scenarios. Climate change is expected to increase the average annual runoff by 15%–38% compared with the base period, and the average annual sediment yield will increase by 4%–32%. The response of runoff and sediment yield varies in different periods, scenarios, and sub-watersheds. Climate-driven vegetation cover changes have an impact on runoff and sediment yield in the watershed, resulting in a difference of 5.8%–12.9% to the total changes. To some extent, the changes in vegetation cover will inhibit the hydrological impact of climate changes. The study helps to clarify the effects of climate and vegetation cover factors on hydrological variations in watersheds and provides further support for understanding future hydrological scenarios and implementing effective protection and use of water and soil resources.

Keywords: climate change; vegetation cover change; GCM; SWAT; runoff; sediment yield

1. Introduction

Climate and vegetation cover change are the foremost drivers of hydrological processes, influencing the water cycle and sediment transport states in watersheds around the world [1,2]. Better understanding of the potential impacts of climate and vegetation cover changes on watershed-scale runoff and sediment yield is critical for long-term water resource planning and management [3].

Since the 20th century, the global environment has changed at an unprecedented rate, which may lead to many environmental problems related to water resources and ecological services [4]. Climate change is undoubtedly the most studied potential driver of hydrological changes, especially in the last decade [5,6]. According to the Intergovernmental Panel on Climate Change (IPCC) report, changes in temperature and precipitation will increase water-related risks, such as floods and droughts [7]. Climate change, by changing the frequency and intensity of precipitation and extreme climatic events and affecting physical processes such as evapotranspiration (ET) and melting of snow and ice, has a wide impact on the spatial and temporal distribution of water and soil resources [8,9]. Thus, it is important to assess the impact of climate change on runoff and sediment yield, which can provide valuable information for the management of water resources and the implementation of land use planning strategies.

Combining general circulation models (GCMs) with hydrological models is the most common method to assess the impact of climate changes on runoff and soil erosion [10,11]. Since different sources of uncertainties, such as internal climatic variability, climate model uncertainty, and scenario uncertainty, are inherent in future climate projections, the use of multiple data sources can appropriately reduce the uncertainties of projections [12]. Bajracharya et al. [13] used the Soil and Water Assessment Tool (SWAT) for assessing the climate change impact on the hydrological regime of the Kaligandaki Basin based on Representative Concentration Pathways Scenarios (RCP 4.5 and RCP 8.5) from the ensemble downscaled Coupled Model Intercomparison Project's (CMIP5) GCM outputs. The results showed that by the end of the 21st century, the increase of annual average temperature and precipitation will lead to significant changes in the hydrological regime, and a 50% increase in discharge is expected at the outlet of the basin. Similarly, Cousino et al. [14] put data from four CMIP5 models into a calibrated SWAT model of the Maumee River watershed to determine the effects of climate change on watershed yields. They found that moderate climate change scenarios reduced annual flow (up to −24%) and sediment (up to −26%) yields, while a more extreme scenario showed smaller flow reductions (up to −10%) and an increase in sediment (up to +11%). It has been widely recognized that climate change will have a significant impact on hydrological processes in many basins around the world [15–17]. Most hydrological response research focuses on the direct impacts of climate change and is usually conducted in conjunction with underlying surface changes. Studies on underlying surface changes generally focus on land use changes caused by human activities, such as urbanization and deforestation lead to changes in land use types [18,19], but rarely involve natural changes in vegetation cover driven by climate change.

Vegetation cover change is another important driver of hydrological variations in watersheds. Vegetation can not only directly affect the water cycle through canopy interception, root absorption and stomatal transpiration, but also impacts various hydrological processes indirectly via the vertical structure and horizontal distribution of the canopy, resulting in the redistribution of water and energy [20,21]. Some recent studies have investigated hydrological responses to vegetation cover changes. Jiao et al. [22] evaluated the impact of vegetation dynamics on hydrological processes in a semi-arid basin using a land surface-hydrology coupled model, and found that vegetation dynamics caused higher ET, lower runoff, and soil moisture content and decelerated the changing trend of discharge. Alvarenga et al. [23] assessed the impact of land cover change on the hydrology of a Brazilian headwater watershed using the Distributed Hydrology-Soil-Vegetation Model, and found that deforestation in forest areas can result in ecosystem soil deterioration, contributing to accelerated erosion, changes in the water dynamics, and a reduction in water availability. Similar results were also found in the Loess Plateau [24] and Yangtze River basin [25]. Although many of these studies have reflected the potential impact of vegetation cover on hydrological processes, the interactions between vegetation and climate change have not been fully considered. How these two factors together affect watershed-scale runoff and sediment yield remains to be further understood.

Numerous recent studies have demonstrated that climate change has an inevitable impact on vegetation growth [26,27]. Most of the research [28,29] shows that there is a close correlation between vegetation cover changes and climate factors (especially temperature and rainfall). Vegetation cover is theoretically a dynamic process due to the influence of long-term climate change [30–32]. Although climate change has a limited impact on vegetation cover in the short term, neglecting the synergy between climate and vegetation cover may reduce the reliability of hydrological modeling when studying the hydrological responses to long-term climate change [33]. Therefore, developing a comprehensive understanding of climate and vegetation cover change factors, will help to predict the trend of various hydrological components in watersheds more accurately, which can provide decision support for the rational use of water resources and reduction of soil erosion under future climate change scenarios.

This study linked climate and vegetation cover change through regression analysis, and then coupled them to a distributed hydrological model (SWAT) for runoff and sediment simulation, aiming at the following research objectives: (1) assessing the direct impacts of climate change on hydrological processes in different periods, and exploring the temporal and spatial dynamics of runoff and sediment yield in watersheds under future climate change scenarios; and (2) analyzing the laws of vegetation cover change driven by climate change, and investigating the potential impacts of vegetation cover change on runoff and sediment process in watersheds. The novelty of the study is to use of various GCMs to cover a wide range of potential outcomes in future climate and take climate-driven vegetation cover change into account for hydrological analysis.

2. Material and Methods

2.1. Study Area

The Zhenjiangguan Watershed (Figure 1) is located in the northern part of Sichuan Province, China, and lies between 103°11′–103°54′ E and 32°9′–33°9′ N. The Zhenjiangguan Watershed is the headstream of the upper Minjiang River, with an area of about 4500 km^2. The watershed has a steep terrain with an altitude of 2325–5537 m and an average elevation of 3610 m. The mountainous climate features of the watershed are obvious, with an average annual temperature of 6.9 °C and an average annual precipitation of 570 mm. The precipitation in flood season (occurring from May to October) accounts for more than 80% of the annual precipitation [34]. Land cover in the Zhenjiangguan Watershed mainly includes grassland and forestland, accounting for 65% and 32%, respectively, and there is a small amount of farmland, bare land, and construction land. The large channel slope and loose soil structure in the watershed make it very sensitive to changes of the natural environment. According to the two recent soil and water loss surveys, the Zhenjiangguan Watershed was significantly affected by hydraulic erosion, and the trend of soil loss may increase in the future [35].

2.2. Data

The Normalized Difference Vegetation Index (NDVI) data used in this study was generated by the product of Moderate-resolution Imaging Spectroradiometer/Normalized Difference Vegetation Index 1-Month (MODND1M), which was provided by International Scientific and Technical Data Mirror Site, Computer Network Information Center, Chinese Academy of Sciences (http://www.gscloud.cn). NDVI is based on the red and near infrared bands to give an estimated greenness, given by:

$$NDVI = (NIR - RED)/(NIR + RED) \tag{1}$$

where *NIR* is the reflectance in the near infrared band and *RED* is the reflectance in the red band. The spatial resolution of MODND1M is 500 m and the temporal resolution is monthly. The time period of monthly NDVI raster data of the study area is from 2000 to 2016. The monthly temperature and precipitation used for NDVI-climate factors regression analysis were extracted from the China Surface Climate Data Day Value Dataset (V3.0), which was obtained from the China Meteorological Data Sharing Service System (http://data.cma.cn).

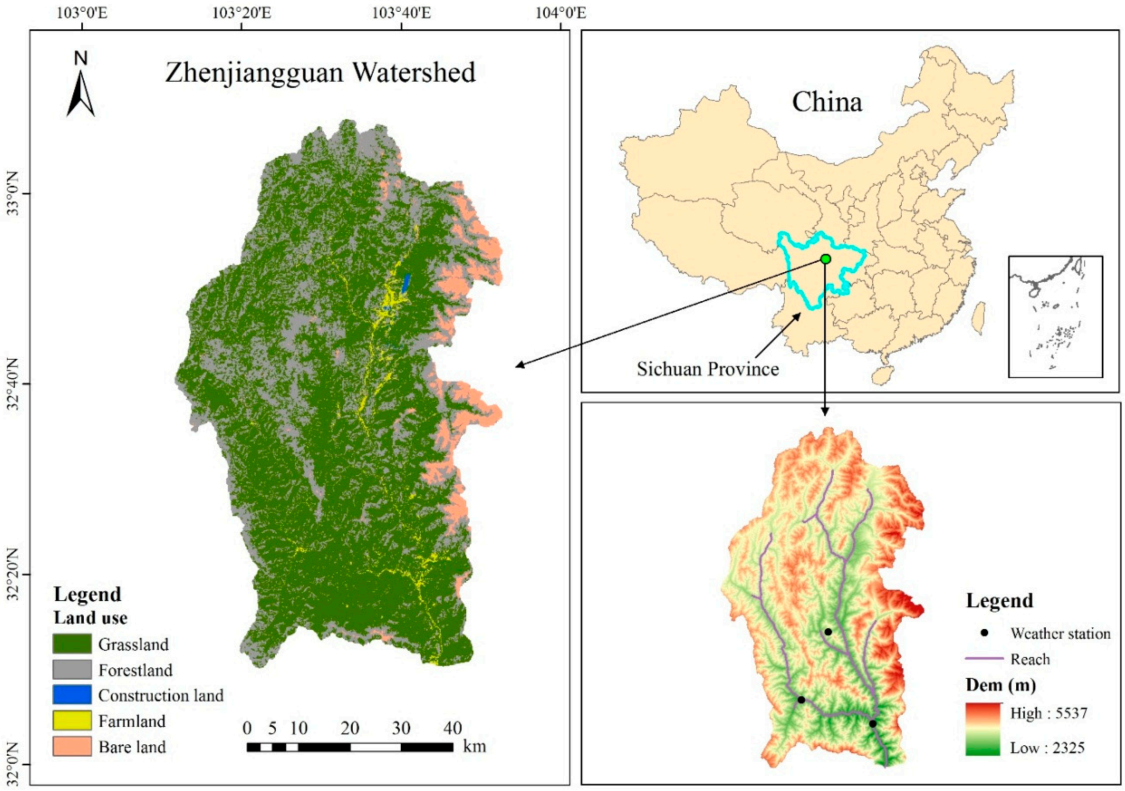

Figure 1. Digital elevation model (DEM), rainfall stations, location, and land use/land cover map for the Zhenjiangguan Watershed.

In the SWAT model, it is necessary to construct a spatial database of elevation, land use and soil type and meteorological data. The elevation data used a digital elevation model (DEM) with a spatial resolution of 30 m provided by the International Scientific and Technical Data Mirror Site, Computer Network Information Center, Chinese Academy of Sciences (http://www.gscloud.cn). A 30 m land use map (2010) of the study area was obtained from the National Earth System Science Data Sharing Infrastructure (http://www.geodata.cn). Soil type and soil attribute information were extracted from 1:1,000,000 China Soil Database, provided by the Cold and Arid Regions Sciences Data Center at Lanzhou (http://westdc.westgis.ac.cn). The historical meteorological data (1978–2005), including daily precipitation, maximum temperature, minimum temperature, wind speed, relative humidity, and solar radiation at three weather stations (Zhenjiangguan, Songpan and Maladun), were provided by the China Meteorological Data Sharing Service System (http://data.cma.cn). Future temperature and precipitation data were generated using projections from three GCMs provided by the Data Distribution Centre of IPCC (http://www.ipcc-data.org).

2.3. Methods

The workflow for this study is shown in Figure 2. First, the GCMs were used to predict climate change data for future periods under different emission scenarios. Then, the NDVI-climate factors regression model was constructed based on historical NDVI remote sensing data and observed temperature and precipitation data, and the future vegetation cover information was updated by combining the future climate projections of GCMs. Finally, the calibrated SWAT model was used to simulate runoff and sediment yield under two different scenarios: changes only in climate and synergistic changes in climate and vegetation cover.

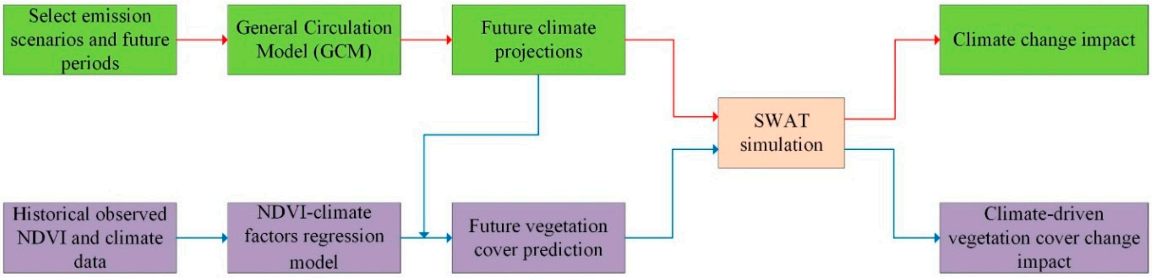

Figure 2. The overall workflow of the study.

2.3.1. Future Climate Projections

Choosing suitable climate models for impact studies is not a straightforward task. Various uncertainties inherent in future climate projections undoubtedly pose major challenges to climate change research. In order to better reflect the possible future climate conditions in the study area, this research used multiple data sources to reveal the predicted differences caused by different emission scenarios and GCMs. Climatic projections from three GCMs (CGCM3 (T47 resolution), CCSM3 and HadCM3) for two emission scenarios (A1B and B1) of the Special Report on Emission Scenarios (SERS) published by the Intergovernmental Panel on Climate Change (IPCC), were used to represent the future climate conditions of the study area. The A1B scenario (medium emission) describes a future world of very rapid economic growth, a global population that peaks in mid-century and declines thereafter, and rapid introduction of new and more efficient technologies. The B1 scenario (low emission) describes a convergent world with the same global population as in the A1B scenario but with rapid changes in economic structures toward a service and information economy, with reductions in material intensity, and the introduction of clean and resource-efficient technologies [36].

Although GCMs are widely regarded as a reliable method for simulating large-scale climate change, they cannot describe the characteristics of regional-scale or watershed-scale climate change well due to their very coarse resolution. Thus, it is essential to downscale the future climate projections of GCMs for use in a hydrological model at a regional or watershed scale. The change factor (CF) is a relatively simple and popular downscaling method for climate change impact assessment. It involves adjusting the observed temperature and precipitation data in watersheds by adding the difference between the future and current temperatures simulated by GCM or multiplying the ratio between simulated future and current precipitation [37]. To quantify the climate change impacts in different time periods, a near-century period (P1) with a time frame of 2020–2039, a mid-century period (P2) with a time frame of 2050–2069, and a late-century period (P3) with a time frame of 2080–2099, were also considered. The data for average monthly precipitation and temperature for the 20th century simulation ($20CM_3$) from 1980 to 1999 and for the emission scenarios (A1B and B1) from the three future periods were collected from the Data Distribution Centre of the IPCC (http://www.ipcc-data.org). The change values for average monthly temperature (absolute change) and average monthly precipitation (relative change) centered on the historical period (1980–1999) and future periods (P1, P2, P3) in different GCMs were then calculated. These GCM changes were used to adjust the observed data (1980–1999) of the meteorological stations within the Zhenjiangguan Watershed to obtain the future climate data for each GCM.

2.3.2. NDVI-Climate Factors Regression Model

The NDVI, which is often used to describe vegetation cover, is the most widely used vegetation index at present [29,38]. Temperature and precipitation are considered the two most important climatic factors affecting vegetation dynamics [30,39], so they were selected for regression analysis with NDVI. Because the responses of vegetation to climate change may vary from one type to another, it is necessary to use the NDVI values of different vegetation types to conduct correlation analysis with climatic factors. The land use types covered by vegetation in the study area mainly included grassland and forestland (accounting for 97% of the total area). The area of farmland was too small to be included in this research.

Many studies have shown that plants are most sensitive to climate change during their vigorous growth period, while they respond slowly to climate change in other periods [27,39]. To more clearly show the response of vegetation growth to climate change, this study focused on the relationship between interannual NDVI and climatic factors (temperature and precipitation) during the growing season (from July to September). The correlation between the NDVI and climate during the growing season was primarily determined by the Pearson correlation coefficient [40], which is computed as:

$$R_{xy} = \frac{\sum_{i=1}^{n}\left[\left(x_i - \overline{X}\right)\left(y_i - \overline{Y}\right)\right]}{\sqrt{\sum_{i=1}^{n}\left(x_i - \overline{X}\right)^2}\sqrt{\sum_{i=1}^{n}\left(y_i - \overline{Y}\right)^2}} \tag{2}$$

where x_i and y_i are the values of data series x and y, respectively; n is the number of the data values; $\overline{X}$ and $\overline{Y}$ are the average values of x and y; R_{xy} is the correlation coefficient between x and y.

Due to the time-lag between changing climate factors and the effect on NDVI [41], the partial correlation coefficients between NDVI and climate variables within the previous four months were calculated. The corresponding monthly interval at which the partial correlation coefficient reached the maximum value was the lag period of the NDVI response to temperature or precipitation.

The NDVI-climate factors regression model was built using IBM Statistical Package for Social Sciences (SPSS), version 20 analysis software (SPSS Inc., Chicago, IL, USA). Mean NDVI values for grassland and forestland in the growing season from 2000 to 2016 were used as the dependent variable, corresponding mean temperature and precipitation were used as independent variables, and the model was built using linear regression. The performance of the established binary linear regression model was evaluated based on the analysis results.

2.3.3. Hydrological Model

SWAT Model

The SWAT is a semi-distributed, continuous-time, and long-term model that can simulate a number of different physical processes such as water, sediment and agricultural chemical yields in large complex watersheds [42]. For SWAT modeling purposes, a watershed may be partitioned into a number of sub-watersheds or sub-basins and then further sub-classified as hydrologic response units (HRU) with a unique grouping of land use, soil and slope [43]. Hydrological simulation at each HRU is performed using the water balance equation:

$$SW_t = SW_0 + \sum_{i=1}^{t}\left(R_{day} - Q_{surf} - E_a - W_{seep} - Q_{gw}\right) \tag{3}$$

where SW_t is the final soil water content (mm H_2O), SW_0 is the initial soil water content on day i (mm H_2O), t is the time (days), R_{day} is the amount of precipitation on day i (mm H_2O), Q_{surf} is the amount of surface runoff on day i (mm H_2O), E_a is the amount of evapotranspiration on day i (mm H_2O), W_{seep} is the amount of water entering the vadose zone from the soil profile on day i (mm H_2O), and Q_{gw} is the amount of return flow on day i (mm H_2O).

The SWAT uses the Modified Universal Soil Loss Equation (MUSLE) to compute soil erosion at HRU level [44], which is expressed as follows:

$$sed = 11.8 \times \left(Q_{surf} \times q_{peak} \times area_{hru}\right)^{0.56} \times K_{USLE} \times C_{USLE} \times P_{USLE} \times LS_{USLE} \times CFRG \tag{4}$$

where sed is the sediment yield on a given day (metric tons), Q_{surf} is the surface runoff volume (mm H_2O/ha), q_{peak} is the peak runoff rate (m^3/s), $area_{hru}$ is the area of the HRU (ha), K_{USLE} is the USLE soil erodibility factor, C_{USLE} is the USLE cover and management factor, P_{USLE} is the USLE support practice factor, LS_{USLE} is the USLE topographic factor and $CFRG$ is the coarse fragment factor.

The plant growth component of SWAT is a simplified version of the Environmental Policy Integrated Climate (EPIC) model [42], and it can simulate leaf area development, interception of light and its conversion into biomass depending on the accumulated heat units. The leaf area development of plants is a function of the growing season and is quantitatively controlled by specific parameters (such as the Leaf Area Index (LAI)) in the plant growth database. The leaf area development plays an important role in the spatial and temporal dynamics of runoff and sediment production and delivery processes in watersheds by affecting physical processes such as evapotranspiration, rainfall interception, and infiltration. In this research, the NDVI obtained from remote sensing data was converted to LAI using an empirical formula [45], and then integrated into the plant growth database of SWAT.

Model Calibration and Validation

The accuracy of SWAT simulations is highly dependent on the calibration and validation procedure. The observed discharge and sediment yields were obtained from the Zhenjiangguan hydrologic station, which was located at the outlet of the whole watershed. The Southern Tibet and Western Yunnan Hydrological Yearbook, which has been examined and verified by the Ministry of Water Resources of the People's Republic of China, have recorded the daily discharge and sediment yields of this hydrologic station over the years. This research extracted the daily discharge and sediment yields from 1985 to 2005, and processed them into monthly values for model calibration and validation. Based on previous research [46,47], the observed data were divided into two parts before running SWAT: one was used for model calibration and the other was used for model validation. The calibration procedure was based on the Sequential Uncertainty Fitting version 2 (SUFI2) algorithm built into the SWAT Calibration and Uncertainty Procedure (SWAT-CUP), which is a semi-automatic calibration method that allows the users to adjust the watershed parameters between auto-calibration runs [48]. To evaluate the performance of SWAT simulation, statistical indicators and graphical analyses were used to compare the simulated and observed discharge and sediment process lines. The following statistical indices were widely used and suggested in SWAT calibration and validation procedure [49–51]: the percentage bias (PBIAS), the coefficient of determination (R^2), and Nash–Sutcliffe (1970) [52] efficiency coefficient (NSE):

$$\text{PBIAS} = \frac{\sum_{i=1}^{n}(Q_{oi} - Q_{si})}{\sum_{i=1}^{n}(Q_{oi})} \times 100\% \tag{5}$$

$$\text{NSE} = 1 - \frac{\sum_{i=1}^{n}(Q_{oi} - Q_{si})^2}{\sum_{i=1}^{n}\left(Q_{oi} - Q_{avg}\right)^2} \tag{6}$$

$$R^2 = \frac{\left[\sum_{i=1}^{n}\left(Q_{oi} - Q_{avg}\right)\left(Q_{si} - Q'_{avg}\right)\right]^2}{\sum_{i=1}^{n}\left(Q_{oi} - Q_{avg}\right)^2 \sum_{i=1}^{n}\left(Q_{si} - Q'_{avg}\right)^2} \tag{7}$$

where n is the number of the data values; Q_{oi} and Q_{si} are the observed and simulated values at month i, respectively; Q_{avg} and Q'_{avg} are the mean values of the observed data and simulated values, respectively. According to the existing research conclusions [50,51], the performance ratings of the model simulation can be classified into four levels (see Table 1).

Table 1. General performance ratings for recommended statistics for a monthly step.

Performance Rating	NSE	R^2	|PBIAS| (%)	
			Discharge	Sediment
Very good	$0.75 < \text{NSE} \le 1.00$	$0.80 < R^2 \le 1.00$	$\lvert\text{PBIAS}\rvert < 10\%$	$\lvert\text{PBIAS}\rvert < 15\%$
Good	$0.65 < \text{NSE} \le 0.75$	$0.70 < R^2 \le 0.80$	$10\% \le \lvert\text{PBIAS}\rvert < 15\%$	$15\% \le \lvert\text{PBIAS}\rvert < 30\%$
Satisfactory	$0.50 < \text{NSE} \le 0.65$	$0.60 < R^2 \le 0.70$	$15\% \le \lvert\text{PBIAS}\rvert < 25\%$	$30\% \le \lvert\text{PBIAS}\rvert < 55\%$
Unsatisfactory	$\text{NSE} \le 0.50$	$R^2 \le 0.60$	$\lvert\text{PBIAS}\rvert \ge 25\%$	$\lvert\text{PBIAS}\rvert \ge 55\%$

3. Results and Discussion

3.1. SWAT Model Calibration and Validation

The observed and simulated monthly discharge and sediment yield during the calibration period (1985–1995) and validation period (1996–2005) are shown in Figures 3 and 4. Table 2 lists the results of the three indices for evaluating model performance.

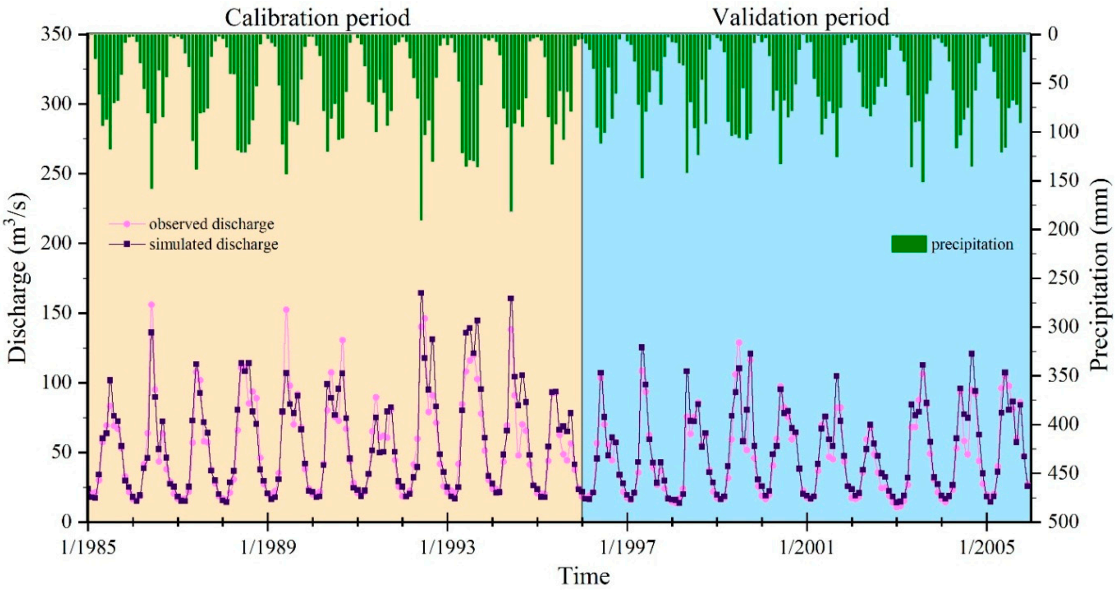

Figure 3. Comparison of observed and simulated values for discharge during the calibration and validation periods.

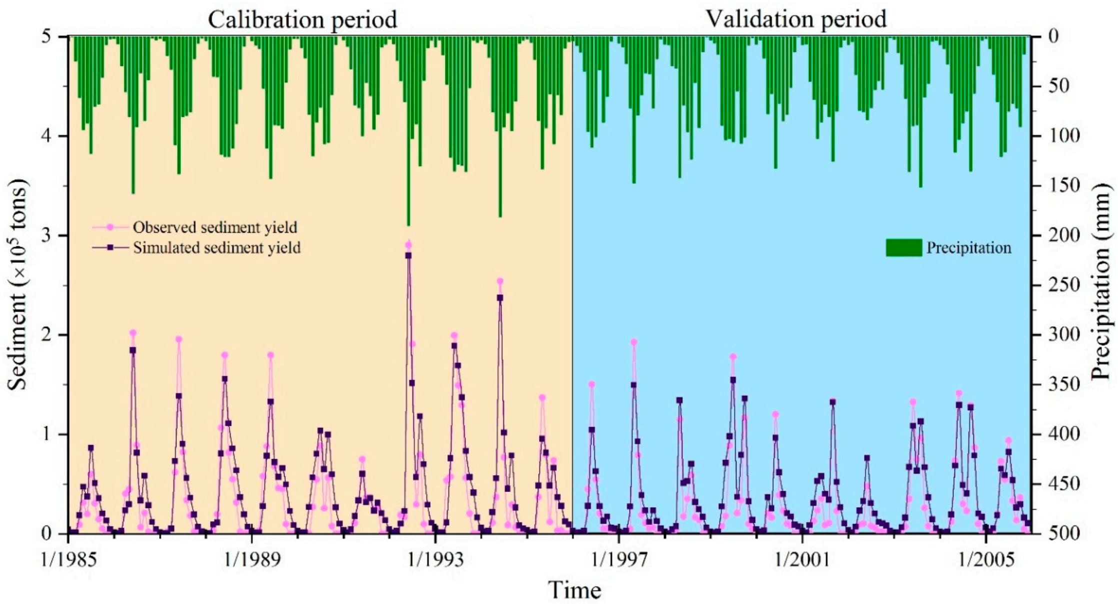

Figure 4. Comparison of observed and simulated values for sediment yield during the calibration and validation periods.

Overall, the fit of observed and simulated values for discharge and sediment yield during calibration and validation periods was relatively high. The statistical indices for discharge simulation during the calibration and validation periods showed "Very good" performance, while sediment simulation showed "Good" performance. This indicated that the calibrated model had high reliability and was suitable for the simulation of runoff and sediment processes in the Zhenjiangguan Watershed.

Table 2. Three evaluation indices of discharge and sediment yield for the calibration and validation periods.

Evaluation Index	Discharge		Sediment Yield	
	Calibration	Validation	Calibration	Validation
PBIAS	4.9%	6.9%	8.2%	10.3%
R^2	0.88	0.87	0.83	0.81
NSE	0.85	0.84	0.72	0.70

3.2. Climate Change Impact

3.2.1. Future Temperature and Precipitation Changes

There were noticeable differences between the projections of different climate models. To reduce the uncertainty of climate change projections, the predicted values of the three GCMs (CGCM3, CCSM3, and HadCM3) were averaged arithmetically in this study. Basin-wide averaged monthly changes of temperature and precipitation, respectively, in three future periods relative to the base period for two emission scenarios (Figure 5) showed that the weather in the Zhenjiangguan Watershed was projected to be warmer and wetter. For the A1B scenario (medium emissions), the annual average temperature in the three future periods was expected to increase by 1.3 °C, 2.2 °C, and 3.0 °C, respectively, compared to the base period. The annual average temperature of the B1 scenario (low emissions) also showed an upward trend, but it was significantly slower than that of the A1B scenario, with rises of 0.9 °C, 1.4 °C, and 2.0 °C in the three future periods. Similarly, compared with the base period, the annual average precipitation under A1B scenario for the three future periods was expected to increase by 12.5%, 19.7%, and 29.6%, respectively, while that under B1 scenario was expected to increase by 14.3%, 23.5%, and 19%, respectively. The increase of precipitation was unevenly distributed in a year, which will further increase the seasonal variation of precipitation in the study area. The increase of precipitation in summer was obvious, which may further aggravate the potential risk of hydraulic soil erosion in the watershed due to the close relationship between rainstorms and erosion and sediment transport. Changes in the frequencies of extreme rainfall events might impinge on land degradation processes, such as soil erosion, removal of top fertile soil, and sand casting, which might reduce agriculture land [13]. The increase of temperature during the year was relatively uniform, with a slightly higher rise in spring and summer. According to Immerzeel et al. [53], higher temperature will increase evapotranspiration and increased melt of ice and snow.

3.2.2. Changes in Runoff and Sediment Yield Caused by Climate Change

Tables 3 and 4 show the simulation results of annual average runoff and sediment yield in the Zhenjiangguan Watershed in three future periods under two emission scenarios, respectively. From the perspective of the changes in different periods of the whole watershed, the annual runoff and sediment yield were projected to be significantly affected by climate change. Compared with the base period (1980–1999), the average annual runoff variation in the three future periods (P1, P2, and P3) ranged from 15% to 38%, and 4% to 32% for sediment yield. The runoff and sediment yield projected for P1, P2, and P3 periods showed a trend of sustained growth, under the A1B scenario. The growth trend of runoff and sediment yield in the P1 and P2 periods under the B1 scenario was roughly the same as that of the A1B scenario, but the growth in the P3 period slowed down. Similar trends also occurred for the changes in precipitation in the future periods, indicating that precipitation changes played a dominant role in runoff and sediment yield. Overall, the difference in runoff and sediment yield between the two scenarios was relatively small in the P1 and P2 periods, but the difference in the P3 period was greater (up to 16% and 24% for runoff and sediment yield, respectively). In the P3 period under the A1B scenario, the growth of runoff and sediment yield reached the highest values (up to 38% and 32%). On the one hand, these were mainly driven by the significant increases of precipitation and higher occurrences of extreme precipitation in summer. On the other hand, the significant increases in spring and winter temperature (>3 °C) led to early snow freshet, thereby increasing runoff and sediment yield significantly. According to the standards for classification and gradation of soil erosion (SL 190–2007) issued by the Ministry of Water Resources of China, the annual average sediment yield in the P3 period under the A1B scenario will reach the "severe" level (>150 t/ha/year), and the soil and water conservation in the watershed will face serious challenges.

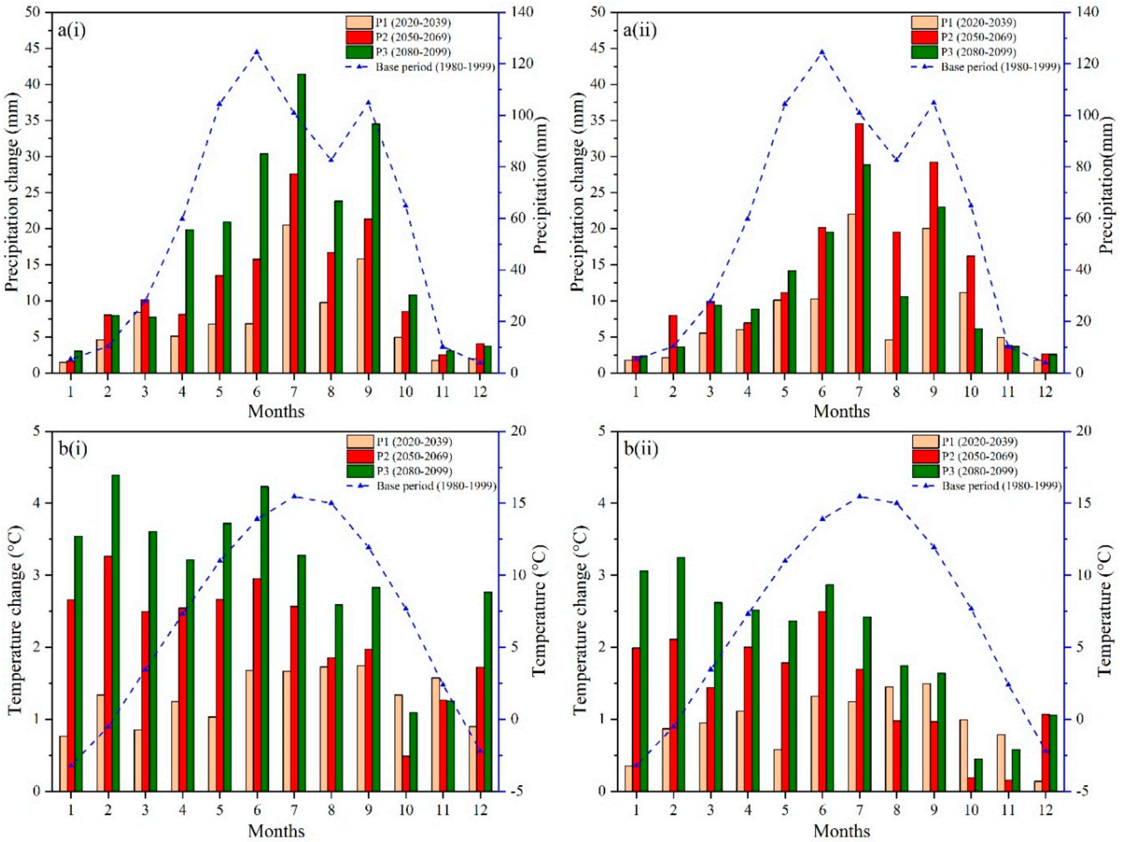

Figure 5. (**a**) Average monthly precipitation changes, and (**b**) average monthly temperature changes between base and three future periods for A1B (**i**) and B1 (**ii**) scenarios.

Table 3. The average annual runoff, and the percentage changes compared with the value of the base period (373 mm), in the three future periods for the A1B and B1 scenarios.

Climate Model	A1B Scenario (mm)			B1 Scenario (mm)		
	P1	P2	P3	P1	P2	P3
T47	430	492	553	448	534	506
HADCM3	442	457	524	425	454	431
CCSM3	417	428	463	419	441	426
Average	430 (15%)	459 (23%)	513 (38%)	431 (16%)	476 (28%)	454 (22%)

Table 4. The average annual sediment yield, and the percentage changes compared with the value of the base period (116 t/ha/year), in the three future periods for the A1B and B1 scenarios.

Climate Model	A1B Scenario (t/ha/year)			B1 Scenario (t/ha/year)		
	P1	P2	P3	P1	P2	P3
T47	126	156	178	128	159	138
HADCM3	119	123	143	119	125	121
CCSM3	117	122	141	118	124	118
Average	121 (4%)	134 (15%)	154 (32%)	122 (5%)	136 (17%)	125 (8%)

Figure 6 shows the annual distribution of runoff and sediment yield in the three future periods under the two emission scenarios. The trends in the annual distribution of runoff are consistent with the baseline period, although there are differences in monthly runoff in different periods. Beginning in January, the monthly runoff gradually increases with the increase of precipitation until the first flood peak appears in June or July. After a month or two, the second flood peak appears in September, and then the monthly runoff gradually declines to the lower levels of the year. There is less consistency in the trend of sediment yield in different periods, and the sediment yield in May and June of the base period is higher than that of the future periods. The difference in future sediment yields mainly occurs in May to September, and the difference in other months is very small. By comparing the monthly average precipitation changes in future periods (Figure 5a), the months with large differences of sediment yield basically coincide with the flood season (usually from May to September). These months are the frequent periods for rainstorms in the Zhenjiangguan Watershed. During the runoff generation stage, rainstorms have a scouring effect on the soil surface, and then a large amount of sediment is transported into the river channel through the confluence process. Therefore, the change of precipitation during the flood season has a dominant impact on the change of sediment yield in the study area.

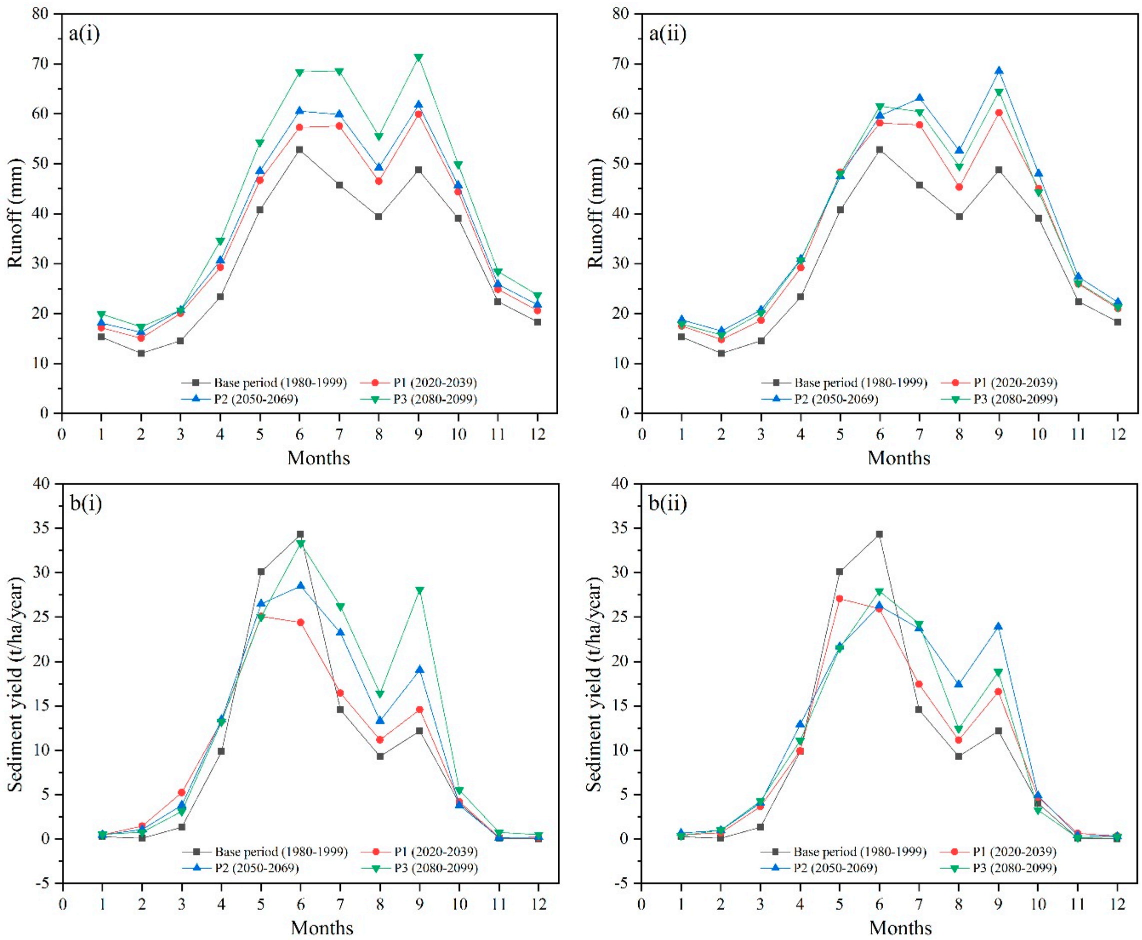

Figure 6. (**a**) Average monthly runoff, and (**b**) average monthly sediment yield in the three future periods for the A1B (**i**) and B1 (**ii**) scenarios.

The average annual runoff and sediment yield (Figure 7) of the 23 sub-watersheds divided by the Zhenjiangguan Watershed in the base period showed significant spatial heterogeneity. These spatial heterogeneities stemmed from the influence of multiple factors such as topography, soil, land cover, and uneven rainfall. The runoff process was obviously affected by topographic factors while the sub-watersheds with steep slopes had a faster collection process for precipitation, which can reduce the water loss caused by evaporation and leakage so it is more conducive to runoff. For sediment yield, besides topography, the effects of soil properties and land cover are equally important. Generally, the sub-watersheds with low topography, a loose soil surface, and sparse vegetation have a greater amount of sediment yield.

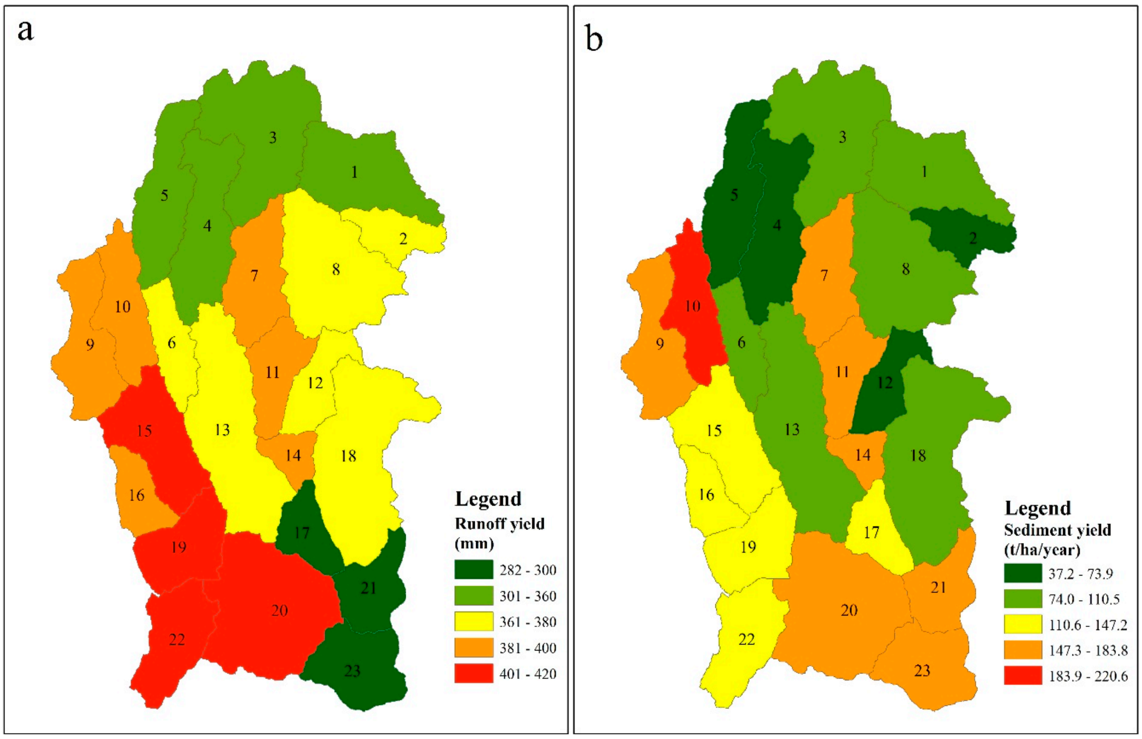

Figure 7. (**a**) Average annual runoff, and (**b**) average sediment yield for each sub-watershed in the base period.

The variations of average annual runoff and sediment yield in the sub-watersheds in the three future periods also showed significant spatial heterogeneity (Figures 8 and 9). Compared with the base period, the runoff in the sub-watersheds increased in all emission scenarios and future periods, with an increase of 12%–42%. In terms of spatial distribution, the variations of average annual runoff in the upstream were larger than that in the downstream. Compared with the base period, most sub-basins had a positive growth in sediment yield, and only a few had negative growth, with overall changes ranging from −24% to 78%. The percentage of runoff and sediment yield changes in different future periods were noticeably different (see Table 5), and the trends of runoff and sediment yield in different periods were consistent with that of the precipitation. The changes in runoff and sediment yield in the P3 period were quite different between the A1B and B1 scenarios, mainly controlled by the significant differences in precipitation and temperature. According to the standards for classification and gradation of soil erosion (SL 190–2007) issued by Ministry of Water Resources of China, a total of 10 sub-watersheds reached the "severe" level of soil erosion in the P3 period under A1B scenario, accounting for 38.2% of the total area. Compared with the base period (15.6%), the area of the watershed affected by severe hydraulic erosion more than doubled.

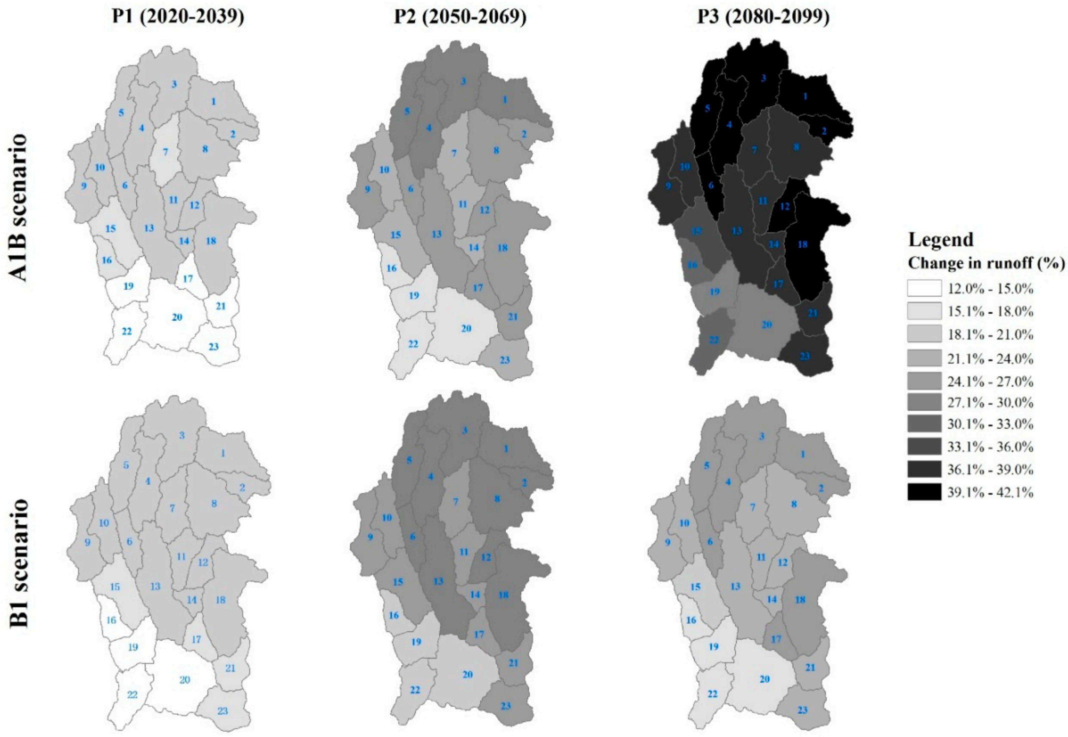

Figure 8. The percentage changes of sub-watershed-scale average annual runoff compared with the value of the base period, in the three future periods for the A1B and B1 scenarios.

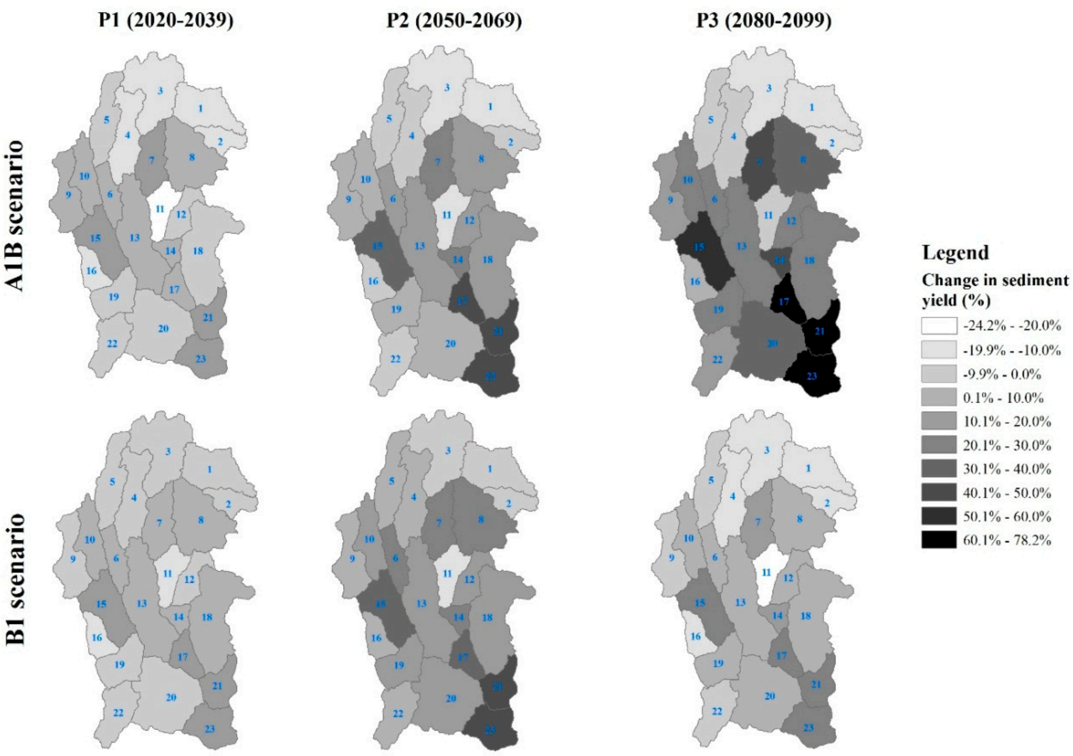

Figure 9. The percentage changes of sub-watershed-scale average annual sediment yield compared with the value of the base period, in the three future periods for the A1B and B1 scenarios.

Table 5. The range of the percentage changes of sub-watershed-scale average annual runoff and sediment yield compared with the value of the base period, in the three future periods for the A1B and B1 scenarios.

	Emission Scenario	Percentage Range (%)		
		P1	P2	P3
Runoff yield	A1B	14–20	15–27	29–42
	B1	14–21	18–30	15–26
Sediment yield	A1B	−21–13	−20–53	−15–78
	B1	−20–17	−15–46	−24–31

3.3. *Effect of Climate-Driven Vegetation Cover Change*

3.3.1. Regression Analysis of NDVI-Climate Factors

The maximum partial correlation coefficient between the average NDVI (July–September) of forestland and grassland and the average temperature and precipitation was for one month prior (see Table 6), indicating that the responses of NDVI to temperature and precipitation changes have a one-month lag period. Therefore, this study selected the average NDVI from July to September in 2000–2016 and the average temperature and precipitation from June to August to construct a regression model. The results of regression analysis are shown in Table 7.

Table 6. Correlation coefficient between average NDVI (July–September) and average temperature and precipitation within four months prior during 2000–2016.

Prior Interval (month)	$R_{NDVI \cdot Temperature}$		$R_{NDVI \cdot Precipitation}$	
	Grassland	Forestland	Grassland	Forestland
0	0.57	0.53	0.45	0.41
1	0.76	0.76	0.67	0.65
2	0.43	0.39	0.20	0.23
3	0.29	0.23	−0.09	−0.10
4	0.08	0.05	−0.19	−0.22
Maximum	0.76	0.76	0.67	0.65

Table 7. The results of regression analysis of NDVI-climate factors.

	Adjusted R^2	Standard Error of Estimate (SEE)	Overall Significance (Sig.F)	Partial Regression Coefficients			Partial Regression Coefficient Significance (Sig.T)	
				Constant	T	P	T	P
Grassland	0.67	0.04	1.7×10^{-4}	−0.32	0.066	0.001	0.003	0.032
Forestland	0.64	0.04	2.9×10^{-4}	−0.13	0.058	0.0008	0.004	0.044

From Table 7, it can be seen that the adjusted coefficients of determination for grassland and forestland were all over 0.6, indicating that NDVI was highly correlated with climate factors, and the change of NDVI can be largely explained by the changes in temperature and precipitation. The standard errors were small, which indicates the observed and estimated values were in good agreement. In variance analysis, the overall F significance measure Sig.F < 0.05 reflects a significant linear relationship between NDVI and temperature and precipitation in the regression model. The partial regression coefficients refer to the regression coefficient corresponding to the constant term and the independent variables (temperature and precipitation) in the regression equation. Sig.T represents the significance of the T-test for partial regression coefficients and having all Sig.T < 0.05 indicates that all independent variables had a significant effect on the dependent variable.

The above analysis results showed that the NDVI-climate factor regression model was of good quality and could be used to predict NDVI values under climate change scenarios. The linear regression equations for NDVI of grassland and forestland, temperature (T), and precipitation (P) were calculated as:

$$\mathrm{NDVI}_{\mathrm{grass}} = 0.066 \times \mathrm{T} + 0.001 \times \mathrm{P} - 0.32 \tag{8}$$

$$\mathrm{NDVI}_{\mathrm{forest}} = 0.058 \times \mathrm{T} + 0.0008 \times \mathrm{P} - 0.13 \tag{9}$$

The above regression equations were used to calculate the NDVI predictions for future climate scenarios, and then the NDVI predictions were converted to the Leaf Area Index (LAI) by an empirical formula [45] and finally added into the plant growth database of SWAT.

3.3.2. Changes in Runoff and Sediment Yield Caused by Vegetation Cover Change

On the basis of keeping the other parameters of the SWAT model unchanged, only the leaf area development parameters corresponding to climate change were adjusted using the NDVI-climate factors regression equations, and then the runoff and sediment simulations in the three future periods under the two emission scenarios were carried out. The contribution of average annual runoff and sediment yield changes caused by vegetation cover changes within the total changes (caused by climate and vegetation synergies) were calculated (see Table 8), reflecting the contribution of vegetation factors to hydrological variation.

Table 8. The percentages of average annual runoff and sediment yield changes caused by vegetation cover changes within the total changes.

	Runoff (%)			**Sediment Yield (%)**		
A1B	P1	P2	P3	P1	P2	P3
T47	−7.3	−9.1	−9.6	−7.1	−9.0	−8.7
HADCM3	−7.1	−12.2	−12.3	−7.0	−11.7	−10.5
CCSM3	−9.3	−14.4	−12.2	−9.0	−13.4	−11.1
Average	−7.9	−11.9	−11.4	−7.7	−11.4	−10.1
B1	P1	P2	P3	P1	P2	P3
T47	−5.1	−8.5	−10.9	−4.9	−8.3	−10.8
HADCM3	−6.6	−10.5	−14.0	−6.4	−10.0	−13.8
CCSM3	−6.5	−12.0	−15.1	−6.1	−11.6	−14.2
Average	−6.1	−10.3	−13.4	−5.8	−10.0	−12.9

The changes of vegetation cover driven by climate change had an impact on runoff and sediment yield in the watershed. According to the SWAT simulation results, the amount of average annual runoff and sediment yield changes caused by vegetation cover changes as a percentage of the total changes ranged from 5.8% to 12.9%, and all were negative. As the weather in the Zhenjiangguan Watershed is projected to be warmer and wetter than the base year (Figure 5), the vegetation cover will increase in future periods according to the regression equations (Equations (8) and (9)). This indicates that the runoff and sediment yield in the watershed are negatively correlated with vegetation cover, and the increase in vegetation cover can effectively reduce the runoff and sediment yield. This is consistent with many previous studies on the influence of vegetation on hydrologic variations [54,55]. Generally, the canopy can act as a water storage system to intercept rainfall and reduce splash erosion by reducing the falling speed of rainwater [20]. Vegetation may also reduce surface water flow velocity and increase infiltration time and infiltration volume, resulting in the increases of surface runoff and soil subsidence in water flow [21]. For evaporation, vegetation transports moisture from soil or even shallow aquifers to the atmosphere through its own transpiration [56]. Therefore, the growth state of vegetation plays a vital role on the spatial and temporal dynamics of runoff and sediment production and transportation.

There is a difference in the influence of vegetation cover change in the three future periods for the A1B and B1 scenarios, and the percentages in the P2 and P3 periods are larger than in the P1 period.

The change of influence mainly comes from the difference of temperature and precipitation in different periods, which in turn affects the key parameter (LAI) in the plant growth database of SWAT. The LAI, which is defined as the area of green leaves per area of land, plays a key role in SWAT for estimating other processes, such as evapotranspiration and biomass accumulation [57]. The LAI determines a series of critical parameters related to runoff and sediment. For instance, the C factor (vegetation cover and management factor) is one of the important factors for simulating sediment yield using the MUSLE in SWAT. The C factor used in SWAT is a function of the amount of residue on the soil surface, which is also obtained from LAI [42]. In addition, parameters such as biomass and the amount of baseflow and surface runoff would be changed if LAI values were adjusted. Therefore, the difference in LAI driven by the change of temperature and precipitation in the future periods is an important reason for the difference in the influence of vegetation on runoff and sediment yield. From the regression equations (Equations (7) and (8)), it can be seen that the partial regression coefficient corresponding to the temperature term is larger than that of the precipitation term, which indicates that the vegetation in the study area is more sensitive to temperature changes. This result is similar to research findings by Chen and Ren [58]. They argue that the vegetation coverage of mainland China is significantly correlated with precipitation and temperature, the correlation with the latter is more significant than with the former. Additionally, Peng et al. [59] also find that the NDVI of Sichuan Province is influenced more significantly by temperature. In SWAT, the plant's growth cycle is based on the heat unit theory, which assumes that plant growth only occurs on the days when daily mean temperature exceeds the base temperature for growth [60]. This means that temperature is the main governing factor for plant growth in SWAT. The significant increase of temperature in the future periods will be beneficial to the increase of LAI in the study area, thus reducing the increase of runoff and sediment yield caused by increased precipitation. Therefore, climate-driven vegetation cover changes will inhibit the effect of climate change on runoff and sediment yield in the study area.

According to most previous studies, climate change is the dominant factor causing hydrologic variations in watersheds, which is also reflected in the simulation results of this study [17,61]. However, compared with only considering climate change factors, there are some differences in hydrological response when considering the climate-driven vegetation cover change factors. According to the case study in the Zhenjiangguan Watershed, the influence of vegetation cover factors on runoff and sediment yield is roughly equivalent to about 10% of climate change. Similarly, a study conducted by Yang et al. [62] in the Luanhe River basin also showed that the increased precipitation is the main driver for the increase in runoff and the increase of vegetation cover may lead to a slight decrease in mean annual runoff. Due to the different research areas and research methods, the influence of vegetation cover on hydrological changes may be quite different. For example, Liu et al. [63] found an equal role of vegetation and climate change on the decline in runoff. Instead of the hydrological modeling approach, they used statistical and elasticity methods and conducted research in a forested catchment in southwestern Australia. Thus, it is meaningful to assess the impact of climate-driven vegetation cover changes based on actual conditions, thereby providing quantitative information for decision-makers to develop healthier water and soil resources planning and management strategies.

It is noticed that the uncertainties involved in climatic models, emission scenarios, downscaling methods, and hydrological models inevitably affect the results of the study. According to Vetter et al. [64], the GCMs are the largest sources of uncertainties in hydrological impact studies, followed by the emission scenarios and hydrological models. Considering the difficulty in evaluating uncertainties in those GCMs, this study mainly focuses on the responses of runoff and sediment yield to various possible climatic conditions in the future and emphasizes the average changes in the analysis. According to Oliveira et al. [65], the use of multiple GCMs and emission scenarios can help to reduce the uncertainties of climate projections. Additionally, uncertainties from different downscaling methods and hydrological models also need to be evaluated further. It should also be noted that the study area is less disturbed by human activities and natural factors (climate and vegetation cover) play a dominant role in the hydrological changes of the Zhenjiangguan Watershed, but this may change with the intensification of human activities in the future. Therefore, hence to examine uncertainty and consider more interfering factors will be the essential objectives of our future work.

4. Conclusions

Based on the SWAT simulation combined with NDVI-climate factors regression analysis, this study assessed the impact of climate and its driven vegetation cover changes on runoff and sediment yield in the Zhenjiangguan Watershed. The main conclusions are as follows:

(1) According to the predictions of GCMs, the future precipitation and temperature in the Zhenjiangguan Watershed showed a significant increasing trend. Compared with the base period, the average annual temperature increase ranged from 0.9 °C to 3.0 °C, and the average annual precipitation increase ranged from 12.5% to 29.6%. Climate change significantly increased the average annual runoff and sediment yield in the three future periods for two emission scenarios (runoff growth 15%–38%, sediment yield growth 4%–32%), and showed significant spatial and temporal heterogeneity. In general, the growth of runoff and sediment yield in the flood season (May–September) was the most obvious, and the variation in runoff and sediment yield differed greatly among the sub-watersheds.

(2) The analysis of the NDVI-climate factors regression model showed that NDVI had a strong correlation with temperature and precipitation in study area, where the adjusted coefficient of determination was over 0.6. The established NDVI-climate factors regression model can be reliably used for NDVI prediction under climate change scenarios.

(3) The climate-driven changes in vegetation cover had an impact on runoff and sediment yield. The runoff and sediment yield in the watershed were negatively correlated with the vegetation cover, showing the increase of vegetation cover can effectively reduce the runoff and sediment yield. The variations of runoff and sediment yield caused by vegetation cover change accounted for 5.8%–12.9% of the total changes, and the climate-driven vegetation cover changes will inhibit the effect of climate change on runoff and sediment yield.

Author Contributions: Conceptualization, S.Z. and Z.L.; Methodology, S.Z. and Z.L.; Software, Z.L.; Validation, S.Z., Z.L. and X.L.; Formal Analysis, S.Z.; Investigation, C.Z. and X.L.; Resources, S.Z.; Data Curation, Z.L.; Writing-Original Draft Preparation, Z.L.; Writing-Review & Editing, S.Z.; Supervision, S.Z. and C.Z.

Funding: This study was supported by the 13th Five-Year National Key Research and Development Program of China (2016YFC0401407) and the Fundamental Research Funds for the Central Universities (2019MS030).

Acknowledgments: The authors thank the International Scientific and Technical Data Mirror Site, Computer Network Information Center, Chinese Academy of Sciences for providing the DEM and NDVI data, the Cold and Arid Regions Sciences Data Center at Lanzhou for providing the soil data, and the China Meteorological Data Sharing Service System for providing the meteorological data. The authors thank Leonie Seabrook, PhD, from Liwen Bianji, Edanz Group China (www.liwenbianji.cn/ac), for editing the English text of a draft of this manuscript.

Conflicts of Interest: The authors declare no conflict of interest.

References

1. Dlamini, N.S.; Kamal, M.R.; Soom, M.A.B.M.; Mohd, M.S.F.B.; Abdullah, A.F.B.; Hin, L.S. Modeling potential impacts of climate change on streamflow using projections of the 5th assessment report for the Bernam River Basin, Malaysia. *Water* **2017**, *9*, 226. [CrossRef]
2. Nilawar, A.P.; Waikar, M.L. Impacts of climate change on streamflow and sediment concentration under RCP 4.5 and 8.5: A case study in Purna river basin, India. *Sci. Total Environ.* **2019**, *650*, 2685–2696. [CrossRef] [PubMed]
3. Li, Z.; Xu, X.; Yu, B.; Xu, C.; Liu, M.; Wang, K. Quantifying the impacts of climate and human activities on water and sediment discharge in a karst region of southwest China. *J. Hydrol.* **2016**, *542*, 836–849. [CrossRef]

4. IPCC (Intergovernmental Panel on Climate Change). Climate Change 2013: The Physical Science Basis. In *Contribution of Working Group I to the Fifth Assessment Report of the Intergovernmental Panel on Climate Change*; Stocker, T.F., Qin, D., Plattner, G.-K., Tignor, M., Allen, S.K., Boschung, J., Nauels, A., Xia, Y., Bex, V., Midgley, P.M., Eds.; Cambridge University Press: Cambridge, UK, 2013; p. 1535.
5. Mishra, Y.; Nakamura, T.; Babel, M.S.; Ninsawat, S.; Ninsawat, S.; Ochi, S. Impact of climate change on water resources of the Bheri River Basin, Nepal. *Water* **2018**, *10*, 220. [CrossRef]
6. Arpe, K.; Hagemann, S.; Jacob, D.; Roeckner, E. The realism of the ECHAM5 models to simulate the hydrological cycle in the Arctic and North European area. *Hydrol. Res.* **2005**, *36*, 349–367. [CrossRef]
7. Min, S.K.; Zhang, X.; Zwiers, F.W.; Hegerl, G.C. Human contribution to more-intense precipitation extremes. *Nature* **2011**, *470*, 378. [CrossRef] [PubMed]
8. Arnone, E.; Pumo, D.; Viola, F.; Noto, L.V.; Loggia, G.L. Rainfall statistics changes in Sicily. *Hydrol. Earth Syst. Sci.* **2013**, *17*, 2449–2458. [CrossRef]
9. Lutz, A.F.; Immerzeel, W.W.; Shrestha, A.B.; Bierkens, M.F.P. Consistent increase in High Asia's runoff due to increasing glacier melt and precipitation. *Nat. Clim. Change* **2014**, *4*, 587. [CrossRef]
10. Lee, S.; Wallace, C.; Sadeghi, A.; McCarty, G.; Zhong, H.; Yeo, I.Y. Impacts of Global Circulation Model (GCM) bias and WXGEN on Modeling Hydrologic Variables. *Water* **2018**, *10*, 764. [CrossRef]
11. Tan, M.L.; Ficklin, D.L.; Ibrahim, A.L.; Yusop, Z. Impacts and uncertainties of climate change on streamflow of the Johor River Basin, Malaysia using a CMIP5 General Circulation Model ensemble. *J. Water Clim. Change* **2014**, *5*, 676–695. [CrossRef]
12. Lutz, A.F.; ter Maat, H.W.; Biemans, H.; Shrestha, A.B.; Wester, P.; Immerzeel, W.W. Selecting representative climate models for climate change impact studies: An advanced envelope-based selection approach. *Int. J. Climatol.* **2016**, *36*, 3988–4005. [CrossRef]
13. Bajracharya, A.R.; Bajracharya, S.R.; Shrestha, A.B.; Maharjan, S.B. Climate change impact assessment on the hydrological regime of the Kaligandaki Basin, Nepal. *Sci. Total Environ.* **2018**, *625*, 837–848. [CrossRef] [PubMed]
14. Cousino, L.K.; Becker, R.H.; Zmijewski, K.A. Modeling the effects of climate change on water, sediment, and nutrient yields from the Maumee River watershed. *J. Hydrol. Reg. Stud.* **2015**, *4*, 762–775. [CrossRef]
15. Zhu, T.; Ringler, C. Climate change impacts on water availability and use in the Limpopo River Basin. *Water* **2012**, *4*, 63–84. [CrossRef]
16. Snyder, K.A.; Evers, L.; Chambers, J.C.; Dunham, J.; Bradford, J.B.; Loik, M.E. Effects of changing climate on the hydrological cycle in cold desert ecosystems of the Great Basin and Columbia Plateau. *Rangel. Ecol. Manag.* **2019**, *72*, 1–12. [CrossRef]
17. Li, F.; Zhang, Y.; Xu, Z.; Teng, J.; Liu, C.; Liu, W.; Mpelasoka, F. The impact of climate change on runoff in the southeastern Tibetan Plateau. *J. Hydrol.* **2013**, *505*, 188–201. [CrossRef]
18. Anand, J.; Gosain, A.K.; Khosa, R. Prediction of land use changes based on Land Change Modeler and attribution of changes in the water balance of Ganga basin to land use change using the SWAT model. *Sci. Total Environ.* **2018**, *644*, 503–519. [CrossRef]
19. Pumo, D.; Arnone, E.; Francipane, A.; Caracciolo, D.; Noto, L.V. Potential implications of climate change and urbanization on watershed hydrology. *J. Hydrol.* **2017**, *554*, 80–99. [CrossRef]
20. Hilker, T.; Lyapustin, A.I.; Tucker, C.J.; Hall, F.G.; Myneni, R.B.; Wang, Y.; Sellers, P.J. Vegetation dynamics and rainfall sensitivity of the Amazon. *Proc. Natl. Acad. Sci. USA* **2014**, *111*, 16041–16046. [CrossRef]
21. Liu, J.; Gao, G.; Wang, S.; Jiao, L.; Wu, X.; Fu, B. The effects of vegetation on runoff and soil loss: Multidimensional structure analysis and scale characteristics. *J. Geogr. Sci.* **2018**, *28*, 59–78. [CrossRef]
22. Jiao, Y.; Lei, H.; Yang, D.; Huang, M.; Liu, D.; Yuan, X. Impact of vegetation dynamics on hydrological processes in a semi-arid basin by using a land surface-hydrology coupled model. *J. Hydrol.* **2017**, *551*, 116–131. [CrossRef]
23. Alvarenga, L.A.; De Mello, C.R.; Colombo, A.; Cuartas, L.A.; Bowling, L.C. Assessment of land cover change on the hydrology of a Brazilian headwater watershed using the Distributed Hydrology-Soil-Vegetation Model. *Catena* **2016**, *143*, 7–17. [CrossRef]
24. Zhang, J.J.; Na, L.; Dong, H.B.; Wang, P. Hydrological response to changes in vegetation covers of small watersheds on the Loess Plateau. *Acta Ecol. Sin.* **2008**, *28*, 3597–3605.

25. Zhao, Y.; Zou, X.; Liu, Q.; Yao, Y.; Li, Y.; Wu, X.; Wang, T. Assessing natural and anthropogenic influences on water discharge and sediment load in the Yangtze River, China. *Sci. Total Environ.* **2017**, *607*, 920–932. [CrossRef] [PubMed]
26. Gao, J.G.; Zhang, Y.L.; Liu, L.S.; Wang, Z.F. Climate change as the major driver of alpine grasslands expansion and contraction: A case study in the Mt. Qomolangma (Everest) National Nature Preserve, southern Tibetan Plateau. *Quat. Int.* **2014**, *336*, 108–116. [CrossRef]
27. Pang, G.; Wang, X.; Yang, M. Using the NDVI to identify variations in, and responses of, vegetation to climate change on the Tibetan Plateau from 1982 to 2012. *Quat. Int.* **2017**, *444*, 87–96. [CrossRef]
28. Liu, H.; Zhang, M.; Lin, Z.; Xu, X. Spatial heterogeneity of the relationship between vegetation dynamics and climate change and their driving forces at multiple time scales in Southwest China. *Agric. For. Meteorol.* **2018**, *256*, 10–21. [CrossRef]
29. Hou, W.; Gao, J.; Wu, S.; Dai, E. Interannual variations in growing-season NDVI and its correlation with climate variables in the southwestern karst region of China. *Remote Sens.* **2015**, *7*, 11105–11124. [CrossRef]
30. Chu, H.; Venevsky, S.; Wu, C.; Wang, M. NDVI-based vegetation dynamics and its response to climate changes at Amur-Heilongjiang River Basin from 1982 to 2015. *Sci. Total Environ.* **2019**, *650*, 2051–2062. [CrossRef]
31. Tong, X.; Wang, K.; Yue, Y.; Brandt, M.; Liu, B.; Zhang, C.; Fensholt, R. Quantifying the effectiveness of ecological restoration projects on long-term vegetation dynamics in the karst regions of Southwest China. *Int. J. Appl. Earth Obs. Geoinf.* **2017**, *54*, 105–113. [CrossRef]
32. Cookson, E.; Hill, D.J.; Lawrence, D. Impacts of long term climate change during the collapse of the Akkadian Empire. *J. Archaeol. Sci.* **2019**, *106*, 1–9. [CrossRef]
33. Zhang, S.; Li, Z.; Hou, X.; Yi, Y. Impacts on watershed-scale runoff and sediment yield resulting from synergetic changes in climate and vegetation. *Catena* **2019**, *179*, 129–138. [CrossRef]
34. Zhang, H.; Li, D.; Jiang, X.; Wang, X. Multiple-scale analysis of runoff-sediment tendency in Zhenjiangguan watershed based on stage characteristics. *J. Hydroelectr. Eng.* **2013**, *3*, 23.
35. Yao, J.; Wang, Y.; Su, W.; Luo, P.N. Fuzzy assessment of ecological vulnerability along upper reaches of Mingjiang River. *Sci. Technol. Manag. Land Resour.* **2006**, *2*, 20.
36. Zhang, L.; Nan, Z.; Yu, W.; Ge, Y. Hydrological responses to land-use change scenarios under constant and changed climatic conditions. *Environ. Manag.* **2016**, *57*, 412–431. [CrossRef] [PubMed]
37. Wang, J.; Nathan, R.; Horne, A.; Peel, M.C.; Wei, Y.; Langford, J. Evaluating four downscaling methods for assessment of climate change impact on ecological indicators. *Environ. Model. Softw.* **2017**, *96*, 68–82. [CrossRef]
38. Rao, Y.; Zhu, X.; Chen, J.; Wang, J. An improved method for producing high spatial-resolution NDVI time series datasets with multi-temporal MODIS NDVI data and Landsat TM/ETM+ images. *Remote Sens.* **2015**, *7*, 7865–7891. [CrossRef]
39. Tang, Z.; Ma, J.; Peng, H.; Wang, S.; Wei, J. Spatiotemporal changes of vegetation and their responses to temperature and precipitation in upper Shiyang River Basin. *Adv. Space Res.* **2017**, *60*, 969–979. [CrossRef]
40. Zhang, Y.; Gao, J.; Liu, L.; Wang, Z.; Ding, M.; Yang, X. NDVI-based vegetation changes and their responses to climate change from 1982 to 2011: A case study in the Koshi River Basin in the middle Himalayas. *Glob. Planet. Change* **2013**, *108*, 139–148. [CrossRef]
41. Paus, A. Human impact, soil erosion, and vegetation response lags to climate change: Challenges for the mid-Scandinavian pollen-based transfer-function temperature reconstructions. *Veg. Hist. Archaeobot.* **2013**, *22*, 269–284. [CrossRef]
42. Neitsch, S.L.; Arnold, J.G.; Kiniry, J.R.; Williams, J.R. *Soil and Water Assessment Tool Theoretical Documentation, Version 2009, Texas Water Resources Institute Technical Report No. 406*; Texas A&M University System College Station: College Station, TX, USA, 2011; pp. 1–647.
43. Flügel, W.A. Delineating hydrological response units by geographical information system analyses for regional hydrological modelling using PRMS/MMS in the drainage basin of the River Bröl, Germany. *Hydrol. Process.* **1995**, *9*, 423–436. [CrossRef]
44. William, J.R. *The EPIC Model. Water Resources Publications*; LLC: Highlands Ranch, CO, USA, 1995; Chapter 25; pp. 909–1000.
45. Li, K.L.; Jiang, J.J.; Mao, R.Z.; Ni, S.X. The modeling of vegetation through leaf area index by means of remote sensing. *Acta Ecol. Sin.* **2005**, *6*, 1491–1495.

46. Arnold, J.G.; Srinivasan, R.; Muttiah, R.S.; Williams, J.R. Large area hydrologic modeling and assessment part I: Model development 1. *J. Am. Water Resour. Assoc.* **1998**, *34*, 73–89. [CrossRef]
47. Thampi, S.G.; Raneesh, K.Y.; Surya, T.V. Influence of scale on SWAT model calibration for streamflow in a river basin in the humid tropics. *Water Resour. Manag.* **2010**, *24*, 4567–4578. [CrossRef]
48. Abbaspour, K.C.; Yang, J.; Maximov, I.; Siber, R.; Bogner, K.; Mieleitner, J.; Srinivasan, R. Modelling hydrology and water quality in the pre-alpine/alpine Thur watershed using SWAT. *J. Hydrol.* **2007**, *333*, 413–430. [CrossRef]
49. Golmohammadi, G.; Rudra, R.; Dickinson, T.; Goel, P.; Veliz, M. Predicting the temporal variation of flow contributing areas using SWAT. *J. Hydrol.* **2017**, *547*, 375–386. [CrossRef]
50. Santhi, C.; Arnold, J.G.; Williams, J.R.; Dugas, W.A.; Srinivasan, R.; Hauck, L.M. Validation of the swat model on a large rwer basin with point and nonpoint sources 1. *J. Am. Water Resour. Assoc.* **2001**, *37*, 1169–1188. [CrossRef]
51. Moriasi, D.N.; Arnold, J.G.; Van Liew, M.W.; Bingner, R.L.; Harmel, R.D.; Veith, T.L. Model evaluation guidelines for systematic quantification of accuracy in watershed simulations. *Trans. ASABE* **2007**, *50*, 885–900. [CrossRef]
52. Nash, J.E.; Sutcliffe, J.V. River flow forecasting through conceptual models part I—A discussion of principles. *J. Hydrol.* **1970**, *10*, 282–290. [CrossRef]
53. Immerzeel, W.W.; Van Beek, L.P.H.; Konz, M.; Shrestha, A.B.; Bierkens, M.F.P. Hydrological response to climate change in a glacierized catchment in the Himalayas. *Clim. Change* **2012**, *110*, 721–736. [CrossRef]
54. Yang, D.; Shao, W.; Yeh, P.J.F.; Yang, H.; Kanae, S.; Oki, T. Impact of vegetation coverage on regional water balance in the nonhumid regions of China. *Water Resour. Res.* **2009**, *45*. [CrossRef]
55. Xu, G.; Zhang, J.; Li, P.; Li, Z.; Lu, K.; Wang, X.; Wang, B. Vegetation restoration projects and their influence on runoff and sediment in China. *Ecol. Indic.* **2018**, *95*, 233–241. [CrossRef]
56. Stephenson, N. Actual evapotranspiration and deficit: Biologically meaningful correlates of vegetation distribution across spatial scales. *J. Biogeogr.* **1998**, *25*, 855–870. [CrossRef]
57. Ma, T.; Duan, Z.; Li, R.; Song, X. Enhancing SWAT with remotely sensed LAI for improved modelling of ecohydrological process in subtropics. *J. Hydrol.* **2019**, *570*, 802–815. [CrossRef]
58. Chen, H.; Ren, Z.Y. Response of vegetation coverage to changes of precipitation and temperature in Chinese mainland. *Bull. Soil Water Conserv.* **2013**, *2*, 18.
59. Peng, W.; Kuang, T.; Tao, S. Quantifying influences of natural factors on vegetation NDVI changes based on geographical detector in Sichuan, western China. *J. Clean. Prod.* **2019**. [CrossRef]
60. Kiniry, J.R.; Macdonald, J.D.; Kemanian, A.R.; Watson, B.; Putz, G.; Prepas, E.E. Plant growth simulation for landscape-scale hydrological modelling. *Hydrolog. Sci. J.* **2008**, *53*, 1030–1042. [CrossRef]
61. Chen, F.; Dudhia, J. Coupling an advanced land surface–hydrology model with the Penn State–NCAR MM5 modeling system. Part I: Model implementation and sensitivity. *Mon. Weather Rev.* **2001**, *129*, 569–585. [CrossRef]
62. Yang, W.; Long, D.; Bai, P. Impacts of future land cover and climate changes on runoff in the mostly afforested river basin in North China. *J. Hydrol.* **2019**, *570*, 201–219. [CrossRef]
63. Liu, N.; Harper, R.J.; Smettem, K.R.J.; Dell, B.; Liu, S. Responses of streamflow to vegetation and climate change in southwestern Australia. *J. Hydrol.* **2019**, *572*, 761–770. [CrossRef]
64. Vetter, T.; Reinhardt, J.; Flörke, M.; van Griensven, A.; Hattermann, F.; Huang, S.; Su, B. Evaluation of sources of uncertainty in projected hydrological changes under climate change in 12 large-scale river basins. *Clim. Change* **2017**, *141*, 419–433. [CrossRef]
65. De Oliveira, V.A.; de Mello, C.R.; Beskow, S.; Viola, M.R.; Srinivasan, R. Modeling the effects of climate change on hydrology and sediment load in a headwater basin in the Brazilian Cerrado biome. *Ecol. Eng.* **2019**, *133*, 20–31. [CrossRef]